COMPUTATIONAL CONTINUUM MECHANICS

ВЫЧИСЛИТЕЛЬНАЯ МЕХАНИКА СЛОШНЫХ СРЕД

Computational Continuum Mechanics. 2021. Vol. 14. No. 2. pp. 144-158 DOI: 10.7242/1999-6691/2021.14.2.12

VALIDATION OF A THERMO-HYDRO-MECHANICAL MODEL FOR FREEZING WATER-SATURATED SOILS BASED ON LABORATORY TESTS

M.S. Zhelnin[1], A.A. Kostina[1], A.E. Prokhorov[1], O.A. Plekhov[1], M.A. Semin[2], K.A. Agutin[3]

[1]*Institute of Continuous Media Mechanics UB RAS, Perm, Russian Federation*
[2]*Mining Institute UB RAS, Perm, Russian Federation*
[3]*Institute of Nature Management of NAS of Belarus, Minsk, Republic of Belarus*

Frost heave of freezing water-saturated soils is one of the main challenges facing engineering today. In regions with cold climates, it causes damage to building and road surfaces foundations. Due to this phenomenon, artificial ground freezing in underground construction projects leads to undesirable uplifting of the soil and increases the lateral ground pressure on the shaft lining and frozen wall. In this paper, a mathematical soil freezing model is proposed to predict soil deformation process occurred due to the phase transformation of pore water into ice. The model is based on a set of nonlinear equations for water transfer, heat transfer and equilibrium, which are solved for porosity, temperature, and displacement variables. The constitutive relations of the poromechanical theory and the effective stress equations (of Bishop type) are used to simulate the mechanical behavior of soil during the process of pore water freezing and to evaluate pore pressure depending on changes in porosity and volumetric strain. In addition, the relations based on the associated plastic flow rule are incorporated into the model to describe the inelastic volumetric expansion of the freezing soil induced by pore ice pressure. The ability of the model to capture essential features of the freezing process of water-saturated soils is demonstrated through the numerical simulations of two laboratory tests. In the first test, the numerical simulation results were compared with the experimental measurements of surface temperature variations and changes that occur in the uplift of the top surface of silty clay specimens with time. It has been shown that the numerical results are highly consistent with the measurements when the soil specimen is frozen with the growth of a massive cryogenic structure. The results of the second test demonstrate that the calculated values of the radial deformation of freezing soil are in good agreement with the experimental measurements obtained by a fiber-optical sensor during the radial freezing of a quartz sand sample in a closed system.

Key words: artificial ground freezing, frost heave, numerical simulation, fiber-optic sensor

1. Introduction

Large-scale development of territories with cold climate is closely related to civil and industrial construction in zones with permafrost and seasonally frozen soil. The freezing process of finely dispersed water-saturated soils is often accompanied by their intensive frost heaving, which entails additional mechanical impact on building foundations [1,2], road surfaces [3,4] and underground pipelines [5,6]. Frost heaving of freezing soils is a problem of increasing importance in the practice of vertical shaft and tunnel sinking by artificial freezing. In this case, the growth of frost heaving forces in the freezing area causes damage to the man-made structures on the ground [7, 9] and increases the ground pressure acting on the ice wall [9] and the shaft lining [10,11]. Thus, the study of the frost heaving phenomenon is an important engineering and scientific direction.

In the Soviet Union, systematic studies in frost heaving of soils began in the 1920s and 1930s with works by M.I. Sumgin, the founder of Russian permafrost studies [12]. M.I. Sumgin proposed a theoretical explanation for the occurrence of volumetric deformation in freezing soil, and also provided experimental evidence for the existence of water movement towards the freezing front in frozen samples. At the same time, S. Taber obtained the results which indicated that the inflow of moisture from an area with a positive temperature is a key mechanism responsible for frost heave in freezing soils [13,14]. Since the 1930s, researchers around the world have concentrated their efforts on identifying patterns between ice formation, moisture migration and frost heaving in freezing soils in order to calculate the vertical displacements of soil during freezing, as well as to assess the effect of frost heaving forces on engineering structures [15–17]. During this period, within the

Email addresses for correspondence: zhelnin.m@icmm.ru

framework of the thermodynamics of phase transitions, of the first thermohydraulic models of freezing soil were developed for describing mathematically the interaction of heat and moisture transfer processes in porous media [18, 19]. On this basis, in the 1970s, a rigid ice model was developed to predict frost heaving in a freezing soil layer taking into account moisture redistribution and formation of ice layers (ice lenses) [20].

Early models were mainly aimed at simulating one-dimensional soil freezing processes: day surface uplifting, and frost heaving effects on foundation beds, and therefore, they lack relations for calculating stresses and strains. However, in geotechnical control associated with for artificial ground freezing, as well as in assessing thermal interaction of an underground pipeline with freezing soil, there is a need to calculate stress and strain field distributions and, consequently, to develop thermo-hydromechanical soil freezing models.

A mathematical basis for describing the mechanical behavior of freezing soil, consistent with thermodynamic principles, is provided by the theory of poromechanics by Coussy [21]. In [22, 23], models have been constructed to take into account the frost swelling phenomenon caused by both the volumetric expansion of crystallized pore water and cryogenic flows, in the process of artificial rock freezing during the construction of tunnels and underground mine design. In these models, freezing soil is assumed to be a poroelastic material, and the ice pressure on the solid skeleton is introduced by means of effective Bishop-type stress. They also include an expression that establishes relationships between changes in porosity, pore pressure, and volume deformations. In turn, the inelastic mechanical behavior of freezing soil is considered [24] within the framework of the thermo-hydro-mechanical model, developed on basis of the Barcelona Basic Model (BBM) for unsaturated soils, which includes two variable stresses: the first is an analogue of the effective stress, and the second is meant to describe the effect of cryogenic suction on the stress-strain state. It was shown that the proposed approach can be used to calculate inelastic tension of soil in the frozen zone occurred due to ice pressure and to predict an increase in shear strength with increasing ice content, as well as to numerically calculate the effect of frost heaving forces on underground pipelines. In [25], the constitutive relations of this model were modified; here the volumetric expansion of freezing soil was represented as elastic and inelastic volumetric deformations, depending on the cryogenic suction variable. However, the developed model was applied only to the in description of mechanical tests of frozen soils.

One-dimensional soil freezing models, derived within the framework of the theory of solid ice, are of great interest from a theoretical point of view [26, 27]. In these models, the stress-strain state is determined through the effective Bishop-type stress, which is calculated analytically by analyzing the dependence of the elastic deformation on the change in the void coefficient. In this case, the soil porosity is calculated by the mass transfer equation. As a criterion for the formation of ice lenses, a condition is hypothesized that the soil porosity exceeds the maximum value established experimentally for each type of soil. The numerical simulation of the laboratory tests on freezing heaving soil performed in [27] showed that the results obtained agree well with the experimentally observed distribution of ice lenses, as well as with measurement values of the sample surface uplift and temperature. At the same time, in contrast to the model of solid ice, the proposed models make it possible to describe the consolidation behavior of unfrozen soil, which is compaction of a water-saturated soil layer with time near the frost front due to the inflow of moisture into the frozen zone.

The results of numerical simulation described in [26, 27] led us to conclusion that the freezing soil porosity calculation according to the mass transfer equation makes it possible to more accurately assess the moisture redistribution in the soil, as well as to estimate its shrinkage ahead of the freezing front due to cryogenic suction, in comparison with other existing models where the mass transfer equation is solved for pore pressure. Moreover, it was shown in [28] that the use of the finite element method to solve the mass transfer equation for pore pressure causes excessive smoothing of the solution near the freezing front, and therefore the calculated value of cryogenic suction is underestimated. However, it should be noted here that the models described in [26, 27] can only be applied to solve problems with unidirectional vertical soil freezing since the calculation of elastic deformation requires analytical

solutions. This factor significantly limits the possibility of their application to engineering problems, especially those associated with the artificial freezing.

In order to overcome this limitation, we propose a modified thermo-hydro-mechanical model for describing the interrelated changes in porosity, pore water and ice pressure, stress and strain fields. The model is based on the constitutive relations of poromechanics with effective Bishop type stress, and the Clausius-Clapeyron equation. It also includes expressions for describing the inelastic volumetric strain induced by pore pressure of ice. The applicability of the model to soil freezing calculations is verified through the numerical simulation of two laboratory experiments. In the first experiment described in [27], the silty clay samples were subjected to one-sided freezing in an open system under various conditions. The second experiment performed by the authors of this study consists in radial freezing of sand in a closed system and includes the mechanical deformation measurements carried out with fiber-optic Bragg grating sensors. Such optical sensors are known to have a fairly high accuracy of measurements, insignificant signal attenuation at long distances, immunity to the effects of electromagnetic fields, and are rather small in size [29, 30]. Due to the listed advantages, fiber-optic sensors are widely used to study the mechanical behavior of soils and concrete, in particular, to analyze soil pressure on supporting structures during the constructions of metro tunnels [31], to measure deformation in soil [32] and concrete [33] exposed to freezing temperatures. Fiber-optic sensors are the key to developing new techniques for controlling water content of soils and to constructing water retention curves [34, 35].

2. Mathematical model of water-saturated soil freezing

Freezing soil is assumed to be a three-phase porous medium composed of solid skeleton (index *s*), fluid water (index *l*) and ice crystals (index *i*). In accordance with recent studies on soil freezing [22, 23, 26, 27], we introduce the following assumptions for constructing a thermo-hydro-mechanical model:

1. Porous medium is initially completely saturated with water, the effects of air and water vapor on moisture soil freezing are not considered;
2. Under freezing, local thermodynamic equilibrium is maintained, and therefore all phases of the porous medium have the same temperature.
3. The freezing point of water does not change, dissolved salts migration and external load are considered insignificant in lowering the freezing point of pore water.
4. Changes in the density of each phase of the porous medium are not considered.
5. Ice motion with respect to solid particles is not taken into account, i.e., ice and solid particles move as a whole.
6. Ice lens formation in the freezing soil is not taken into account.
7. The solid skeleton of the porous medium is assumed to be isotropic.
8. Deformations of a porous medium during moisture freezing are described within the framework of the theory of small deformations.

We consider two zones in the porous medium. The temperature in one of these regions (we call it a frozen zone) is below the pore water freezing point; this zone contains soil particles, ice and fluid water. In this frozen zone, we distinguish an area (a frost penetration region) with cryogenic flows. Another zone where the temperature is higher than the water freezing point is termed an unfrozen zone; it contains only soil particles and fluid water.

The system of equations for describing freezing soil includes:

– equation for mass transfer

$$\frac{\partial\left(\rho_l S_l n\right)}{\partial t}+\frac{\partial\left(\rho_i S_i n\right)}{\partial t}+\operatorname{div}\left(\rho_l \mathbf{v}_l\right)=0; \qquad (1)$$

– equation for heat transfer

$$C\frac{\partial T}{\partial t} - \mathrm{div}\lambda\,\mathrm{grad}T + C_l\mathbf{v}_l\cdot\mathrm{grad}T = Q_{ph}; \qquad (2)$$

– equilibrium equation

$$\mathrm{div}\,\boldsymbol{\sigma} + \boldsymbol{\gamma} = 0. \qquad (3)$$

The following symbols are used in writing Eqs. (1-3): $\rho_j S_j n$ - water ($j = l$) and ice ($j = i$) content at initial time t; ρ_j — density and S_j — phase saturation j; n — porosity; C_l, $\mathbf{v}_l$ — volume heat capacity of water and its velocity with respect to the solid skeleton; $\boldsymbol{\sigma}$ —total stress tensor; $\boldsymbol{\gamma}$ — specific weight of the porous medium; T — temperature; C — volumetric hat capacity and λ — thermal conductivity of the porous medium; Q_{ph} — heat source caused by the latent heat released in the phase shift during water crystallization.

In the mass balance equation (1), the ice saturation S_i is a power function of temperature, which is expressed as

$$S_i = \begin{cases} 1-\left[1-\left(T-T_{ph}\right)\right]^{\alpha}, & T \le T_{ph}, \\ 0, & T > T_{ph}, \end{cases}$$

where T_{ph} is the pore water freezing point, and α is the parameter found experimentally.

From the complete saturation condition it follows that the water saturation S_l can be expressed as: $S_l = 1 - S_i$ .In (1), the water velocity with respect to the solid skeleton is given by Darcy's law

$$\mathbf{v}_l = -k\,\mathrm{grad}\,\psi,$$

where k is the water saturation ratio, and ψ is the soil water potential. The thermal conductivity ratio k is expressed as power function of temperature T [36]:

$$k = \begin{cases} k_0\left[1-(T-T_{ph})\right]^{\beta}, & T \le T_{ph}, \\ k_0, & T > T_{ph}, \end{cases},$$

where k_0 is the moisture permeability coefficient of unfrozen soil, β is the parameter determined experimentally. The potential of soil moisture ψ is defined as

$$\psi = \frac{p_l}{\rho_l g} + z,$$

where p_l is the pore-water pressure, g is the acceleration of gravity, and z is the vertical coordinate.

In order to find the value of pore-water pressure, following [26] and [27], we use the Clausius-Clapeyron equation and the Bishop relation for effective pore pressure in the frozen zone. Thus, the water pressure can be written as

$$p_l = \frac{(1-\chi)(\rho_l - \rho_i)\, p_0 + (1-\chi)\rho_l\rho_i L \ln\left(T/T_{ph}\right) + \rho_l p}{\chi\rho_l + (1-\chi)\rho_i},$$

where L is the specific heat of water crystallization, p_0 is the initial pore-water pressure, and χ is the pore pressure parameter dependent on the water saturation S_i:

$$\chi = (1-S_i)^{1,5}.$$

In the heat transfer equation (2), the phase-induced volume source takes the form

$$Q_{ph} = L\rho_i \frac{\partial(nS_i)}{\partial t}.$$

The volume heat capacity C and heat conductivity λ are calculated as in [38]

$$C = (1-n)c_s\rho_s + nS_l c_l\rho_l + nS_i c_i\rho_i,$$
$$\lambda = \lambda_s^{1-n}\lambda_l^{nS_l}\lambda_i^{nS_i},$$

where c_j, λ_j are the specific heat capacity and heat conductivity of the phase j ($j = s,l,i$).
In the equilibrium equation (3), the total stress tensor $\boldsymbol{\sigma}$ is written as [21]:

$$\boldsymbol{\sigma} = \boldsymbol{\sigma}' - b(p - p_0)\mathbf{I}, \qquad (4)$$

where $\boldsymbol{\sigma}'$ is the effective stress tensor, p_{por} is the pore pressure, b is the effective Biot coefficient, $\mathbf{I}$ is the unit vector. For isotropic material, the effective stress tensor $\boldsymbol{\sigma}'$ is calculated according to Hook's law:

$$\boldsymbol{\sigma}' = \left(K - \frac{2}{3}G\right)\varepsilon_{vol}^{el}\mathbf{I} + 2G\boldsymbol{\varepsilon}^{el},$$

where K is the effective volumetric modulus, G is the effective shear modulus, $\boldsymbol{\varepsilon}^{el}$ is the elastic strain tensor, and ε_{vol}^{el} is the volumetric elastic strain.
Based on the principle of additive decomposition of the total strain tensor $\boldsymbol{\varepsilon}$, the elastic strain tensor $\boldsymbol{\varepsilon}^{el}$ can be expressed as

$$\boldsymbol{\varepsilon}^{el} = \boldsymbol{\varepsilon} - \boldsymbol{\varepsilon}^{th} - \boldsymbol{\varepsilon}^{in},$$

where $\boldsymbol{\varepsilon}^{th}$ is the thermal expansion tensor, and $\boldsymbol{\varepsilon}^{in}$ is the inelastic strain tensor. In this case, the total strain tensor $\boldsymbol{\varepsilon}$ is found from the geometric relation of the small deformation theory.

$$\boldsymbol{\varepsilon} = \frac{1}{2}\left(\operatorname{grad}\mathbf{u} + \operatorname{grad}\mathbf{u}^{\mathrm{T}}\right),$$

where $\mathbf{u}$ the displacement vector. The thermal expansion tensor, is written in the form

$$\boldsymbol{\varepsilon}^{th} = \alpha_T \left(T - T_0\right)\mathbf{I},$$

where α_T is the thermal expansion coefficient, and T_0 is the initial temperature of unfrozen soil. The pore pressure p is found using the expression of the theory of poromechanics [21]. Thus, we get

$$p = p_0 + N\left(n - n_0 - b\varepsilon_{vol}^{el} + 3\alpha_T\left(b - n_0\right)\left(T - T_0\right)\right), \quad (5)$$

where n_0 is the initial porosity, and N is the effective tangent Biot modulus.

Effective mechanical parameters are determined by the formula [22]:

$$X = S_i X_{fr} + S_l X_{un},$$

where X is the effective parameter value, and X_{fr} and X_{un} are the values of parameters for both frozen and un-frozen soil zones.

Freezing may cause significant volume expansion of the soil in the frozen zone under the action of frost heaving forces. The use of only constitutive relations of poroelasticity can lead to a maximum overestimation of the average effective stress in the frozen zone. A more realistic description of the stress-strain state of a freezing soil can be achieved if we assume the inelastic mechanical behavior of a solid skeleton under tension studied in tensile tests. In accordance with [24], inelastic volumetric deformation occurs if, under the influence of pore pressure of ice, the average effective stress exceeds the tensile strength of the rigid skeleton. In [25], lastic and inelastic components of volumetric deformation are additionally introduced, which depend on cryosuction. In this case, inelastic volumetric deformation occurs when the value of cryosuction exceeds its threshold limit, which depend on the type of soil.

According to this approach, the model additionally includes the inelastic volumetric deformation $\boldsymbol{\varepsilon}^{fh}$, caused by frost heaving forces.

$$\boldsymbol{\varepsilon}^{fh} = \varepsilon_{vol}^{fh}\mathbf{I},$$

where ε_{vol}^{fh} is the value of inelastic volumetric deformation of soil . As a condition for the onset of the inelastic volumetric deformation, the following yield criterion is used

$$F = A\sigma'_m - B,$$

where σ'_m is the effective mean stress. The coefficients A and B are defined as in the Drucker – Prager yield criterion:

$$A = \frac{6c\cos\varphi}{\sqrt{3}\left(3 - \sin\varphi\right)}, \qquad B = \frac{2\sin\varphi}{\sqrt{3}\left(3 - \sin\varphi\right)},$$

where c is the coefficient of particle adhesion in unfrozen soil, and φ is the angle of internal friction of unfrozen soil. The calculation of the inelastic volumetric deformation $\boldsymbol{\varepsilon}^{fh}$ is performed using the yield function F based on the associated rule of plastic flow.

Thus, the inelastic volumetric deformation $\boldsymbol{\varepsilon}^{fh}$ in frozen soil occurs because the effective mean stress σ'_m exceeds the tensile strength of the solid skeleton. According to expression (5), the pore pressure p is determined by the porosity n of the soil , and therefore the growth of porosity in the frozen zone due to the volume expansion of the freezing pore water and due to the flow of additional

water from the side of the non-frozen zone increases the pore pressure p, which, in , makes the stress σ'_m higher, which follows from relation (4). Note that the volumetric deformation $\boldsymbol{\varepsilon}^{fh}$ describes only the volumetric expansion of the soil, which is associated with the formation of a massive cryogenic structure, i.e., in the absence of thick ice lenses. If the freezing process of the soil is accompanied by an intensive ice segregation with thick ice lenses formation, then fractures in the soil skeleton are generated. In this case other approaches, for example based on the ice rigid theory, can be used.

Nonlinear differential equations of mass transfer (1), heat transfer (2) and equilibrium (3) equations were implemented in Comsol Multiphysics®. The mass transfer equation was introduced into the package with a Weak Form PDE interface, which allows discretizing the problem via weak formulation using the chosen basis functions. The heat transfer and solid mechanics equations were solved by applying the heat transfer and solid mechanics modules. Porosity n, temperature T and displacement vector $\mathbf{u}$ were treated as unknown field variables determined from the numerical solution of equations (1) - (3). Spatial discretization of the equations was carried out by the finite element method. Porosity n and temperature T were approximated by the linear Lagrange polynomials, and displacement $\mathbf{u}$ - by the quadratic Lagrange polynomials. Time discretization was carried out on the basis of the implicit Euler scheme. A discrete analogue of the original problem, which is a system of nonlinear algebraic equations, was solved numerically using Newton's method.

3. Results of numerical simulation

To verify the efficacy and performance of the developed thermo-hydromechanical model in case of the freezing process of moisture-saturated soils, we have simulated numerically two laboratory experiments. The results of the first experiment, one-sided freezing of silty clay samples in an open system, were taken from [27]. The second experiment was carried out by the authors of this article. In this experiment, the deformation of sand during its radial freezing was investigated using fiber-optic sensors.

3.1. Numerical simulation of one-side freezing test (test 1)

In laboratory test 1, which was carried out by Y. Lai et al. [27], one-sided artificial freezing of cylindrical silty clay samples (10 cm in diameter and height) was implemented in an open system. Negative and positive temperatures were maintained constant at their upper and lower ends of the samples. The water flow was supplied to the lower end of each sample. The lateral surfaces of the samples were thermally insulated. This research was chosen due to the fact that the one-dimensional thermo-hydromechanical model of soil freezing presented in it served as the basis for constructing the model described in Section 2.

By performing numerical simulation, we have considered two freezing modes. In the first regime, the temperature was maintained negative ($T_{fr} = -1,6\,^\circ\text{C}$) at the upper end of the samples, and positive ($T_w = 1,0\,^\circ\text{C}$) at their lower ends. In the second regime, the freezing temperature $T_{fr} = -1,6\,^\circ\text{C}$ was -4.0°C at the upper end, and $T_w = 1,5\,^\circ\text{C}$ was maintained at the lower end. In both regimes, the external axial load P_{ob}, i.e. 50 and 100 kPa, respectively, was exerted on both ends.

The experimental conditions ensured the unidirectional freezing of soil samples from the upper to the lower end. On this basis, the computational domain was a rectangle that coincided with half of the axial cross-section of the cylinder, which was divided into 620 quadrangular elements. The optimal size of the computational grid was determined from the grid convergence analysis.

As mentioned before, the temperature T_{fr} and the porosity n_b at the rectangle edge are equal. According to [26], it was assumed that at the beginning of freezing, the pore moisture contained in the soil at the upper end of the sample quickly crystallizes into ice in the absence of the flow of additional moisture from the non-frozen zone. Since the volume of the crystallized water increases by approximately 9%, the value of soil porosity at the upper end increases by a factor of 1.09

compared to the initial value. As a result, the porosity n_b was $1{,}09n_0$, where n_0 is the initial porosity. Constant positive temperature and initial porosity were maintained at the lower boundary of the computational domain because, in this experiment, the inflow of water was provided to the lower end of the sample. On the rectangle side corresponding to the external cylindrical surface of the samples, the heat and mass fluxes were assumed to be zero. The symmetry condition was imposed on the side of the rectangle coinciding with the axis of the samples. To calculate the stress-strain state of the soil during freezing, a vertical load P_{ob} was applied to the upper boundary of the rectangle, the movement on the lateral sides of the rectangle was permitted only in the vertical direction (along the axis z), and the movement on the lower boundary was restricted in all directions.

The initial temperature of the sample T_0 was equal to 3.0°C in the first freezing mode and to 2.6°C in the second. Thermophysical parameters for water and ice are given in Table 1. Material parameters for silty clay are presented in Table 2. The values of thermophysical and elastic characteristics were taken from [27]. The missing parameters of the model were determined by carrying out a sequential series of calculations.

Table 1. Thermophysical characteristics of ice and water

ρ_l, кг/м^3	λ_l, Вт/(м·К)	c_l, кДж/(кг·К)	ρ_i, кг/м^3	λ_i, Вт/(м·К)	c_i, кДж/(кг·К)	L, кДж/кг
1000	0,58	4,18	917	2,22	2,043	334,56

Table 2. Material parameters for silty clay

n_0, м^3/м^3	ρ_s, кг/м^3	λ_s, Вт/(м·К)	c_s, Дж/(кг·К)	k_0, м/с	α	β	α_T, 1/К	c, кПа
0,32	2360	1,5	1000	$1{,}58\cdot10^{-10}$	–3,0	–3,8	$2{,}0\cdot10^{-6}$	14,0
φ, град	K_{un}, МПа	G_{un}, МПа	N_{un}, МПа	b_{un}	K_{fr}, МПа	G_{fr}, МПа	N_{fr}, МПа	b_{fr}
18	2,75	1,05	18,4	0,75	8,60	3,30	18,7	0,73

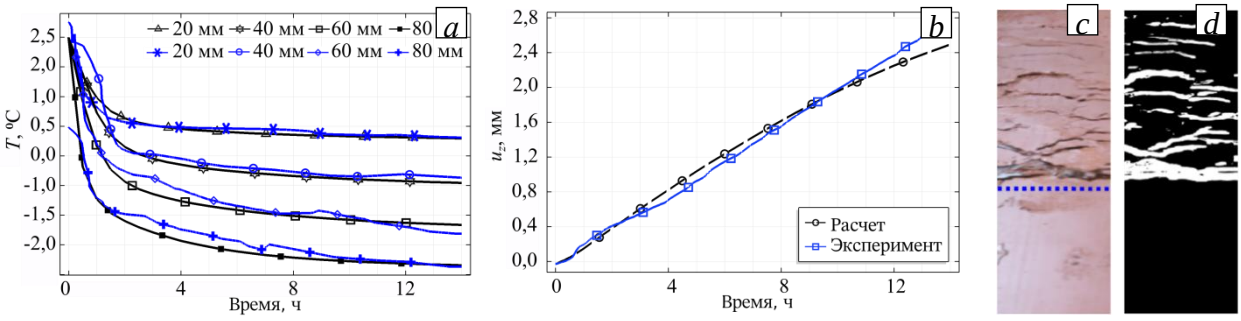

Fig.1. First freezing regime: (a) Calculated versus experimental values graphs showing how the temperature changes with time at the points inside the sample at heights 20, 40, 60, 80 mm from the lower end of the sample (upper markers – calculated curves) and (b) the curves for the vertical displacement u_z of the upper end of the sample at $P_{ob} = 50$ kPa ; (c) silty clay sample with ice lenses and (d) its binary model (images are taken from [27]).

Figure 1 presents the graphs of temperature versus time for the internal points of the samples and the graphs of the vertical displacement u_z of the upper end, which were plotted by analyzing the results of the numerical simulation of sample artificial freezing in the first temperature regime. The data were obtained during the time interval of 14 hours, after which the temperature of the sample stabilized, and the increase in displacement u_z occurred only due to an increase in the thickness of the final ice lens near the freezing front.

From the temperature evolution graphs presented in Figure 1a, it can be seen that, in the first 2 hours of freezing, the temperature drops rapidly at all points under consideration and then it decreases gradually to the lowest possible values. Due to the low freezing temperature ($T_{fr} = -1,6$ °C), the temperature transition below 0°C occurs only at two points: at 60 and 80 mm heights near the upper end of the sample. The process of soil freezing at these points proceeds smoothly, with a gradual phase transition of pore moisture into ice. For two other points, at 20 and 40 mm heights, located closer to the lower end, the temperature stabilizes faster, which is caused by more intensive compensation for heat loss due to the heat gain from the unfrozen soil.

The variations in measurements are observed at the points at 60 and 80 mm heights; the difference between the calculated temperature and the experimental data is maximum. The experimental curves passing through the points located at some distance to the upper end exhibit smaller fluctuations. For these points, there is a minimal discrepancy between the calculated and experimental curves showing how the temperature variation changes with time.

It is seen (Fig. 1b) that the curve illustrating the change in the vertical movement of the upper end rises monotonically. Hence, it follows that the freezing is accompanied by a volumetric expansion of the soil, caused by frost heaving due to the phase transition of water into ice and an additional water flow from the side of the lower end of the sample. The magnitude of displacement obtained via numerical simulations is in good agreement with the experimental measurements recorded over the period of 10 hours. After that, the calculated value of displacement becomes less than the measured value due to the fact that the thickness of the final ice lens increases significantly, which cannot be described in the framework of the developed model (Fig. 1c).

Similar results for the second freezing regime are shown in Figure 2. As in the previous case, the data are given until the temperature stabilizes (over 20 hours). In the second regime, unlike the first one, the temperatures at the points inside the sample stabilize more slowly, which is associated with soil freezing to a greater depth at high freezing temperature: $T_{fr} = -4,0$ °C ° C. Also, in this

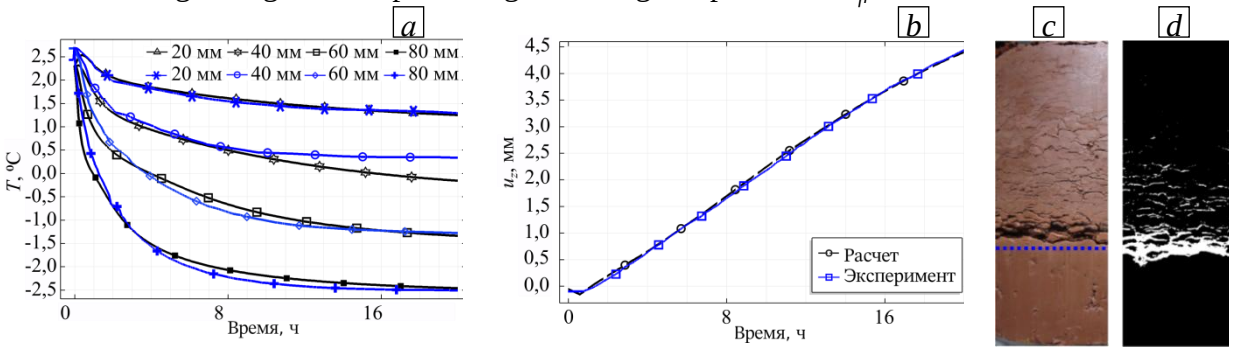

Fig.2. Second freezing regime: (a) calculated versus experimental values graphs showing how the temperature changes with time at the points inside the sample located at 20, 40, 60, 80 mm heights from its lower end (upper markers – calculated curves) and (b) the curves for the vertical displacement u_z of the upper end of the sample at $P_{ob} = 50$ kPa ; (c) silty clay sample with ice lenses and (d) its binary model (images are taken from [27]).

case, the graphs depicting the temporal evolution of the temperature and plotted for the points in the vicinity of the upper end of the sample at 60 and 80 mm heights are in better agreement with the experimental curves. This can be related to an increase in the intensity of freezing, which contributes to less temperature fluctuations and faster ice formation without significant overcooling of the water. The greatest deviation of the calculated temperature from the measured one is

observed for the point at a distance of 40 mm from the upper end of the sample. Note that the calculated temperature gradually decreases with time, while, in the experiment, it quickly stabilizes.

When the soil is frozen at a lower temperature and under a higher vertical load, this, on the one hand, accelerates its freezing and, on the other, causes a massive cryogenic structure without thick ice lenses to occur in it. The comparison of the curves given in Fig.2b leads us to conclude that, in this case, the calculated time dependence of the vertical displacement quite accurately coincides exactly with that constructed from the experimental data. The curve segment (both curves) within which the displacement u_z remains constant and which indicates that the frost heaving is controlled by an external vertical load corresponds to the first hour of freezing. After the frost heaving forces exceed the external load, the displacement increases monotonically. Upon completion of 20 hour freezing, the final ice lens appears in the sample and therefore no further numerical modeling is carried out.

The character of soil freezing with massive ice formation without thick ice lenses, which is observed in the second freezing regime until the temperature stabilizes in the sample (Fig. 2c), is in good agreement with the assumptions made during the development of the model. The comparison of the results of numerical simulation with the experimental data shows that, under these conditions, the model is able to accurately describe (with a maximum deviation of less than 0.07 mm) an increase in the height of a frozen sample due to frost heaving. At the same time, the results of numerical modeling of the slow freezing of the soil sample at a low freezing temperature predict an underestimated displacement of the upper end of the sample with a maximum deviation of less than 0.26 mm, which is due to the formation of thick ice slips (Fig. 1c). For both freezing modes, the calculated time variation of temperature inside the samples is in acceptable (with a deviation of no more than 0.35°C in the frozen zone) agreement with the measurements.

3.2. Numerical simulation of radial freezing (test 2)

In Section 3.1, we describe an artificial freezing experiment performed on the samples made of silty clay, which is characterized by the intense cryogenic suction-induced migration of moisture into the frozen zone. However, in many geotechnical problems related to underground construction in difficult hydrogeological conditions, there occurs a need for artificial freezing of watered sandy soils. Sandy soils consist of larger, in comparison with clays, mineral particles, and thus their frost heaving is mainly caused by the volumetric expansion of freezing water initially contained in the pore space. The moisture movement towards the freezing front proceeds very slowly or completely absent.

In order to assess the capability of the model to describe soil deformation under the frost heaving forces caused by the volumetric expansion of water during its phase transition into ice, a numerical simulation of an experiment on the radial freezing of water-saturated quartz sand in a closed system was performed. Let us consider the key features of test 2.

The sand saturated with distilled water was placed in a rigid plastic container 1 in the form of a cylinder with a wall thickness of 28 mm (Fig. 3a). The container was closed from below and from above with 2 mm thick lids. A copper tube 2 was installed along the container axis. The resulting soil sample after packing the sand was ultimately a hollow cylinder 5 mm high with internal and external radii of 10 and 57 mm, respectively. In the radial soil freezing test, a coolant was circulating through a copper tube (Fig. 3b). The cooling system consisted of a thermally insulated box, a freezer, an expansion tank and a pump. During the experiment, a plastic container with sand was placed inside a thermally insulated chamber to protect the soil from the external heat influx from the environment. A copper tube in the center of the container was attached to the pump and the expansion tank filled with refrigerant. The expansion tank was installed inside the freezer, where a constant temperature of about –30 ° C was maintained. The pump circulated the refrigerant through the copper tube.

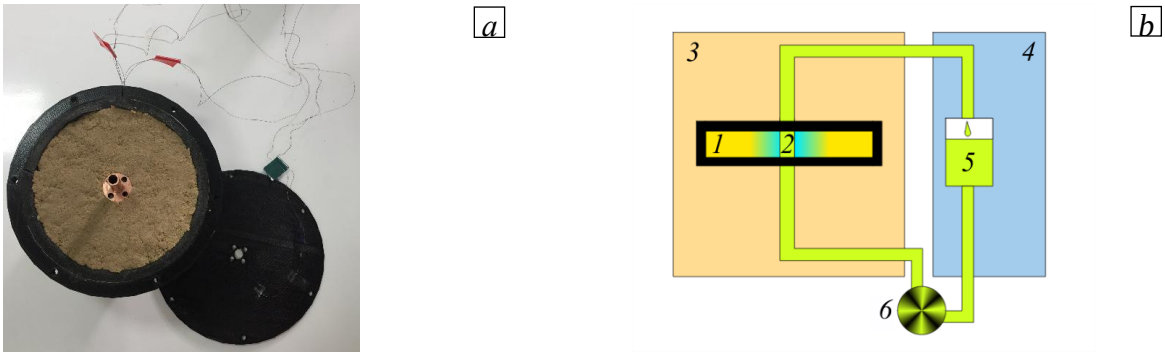

Fig.3. Top view photos of the plastic container filled with water-saturated sand (a); design scheme for the cooling system (b); container with sand (1), copper tube (2), thermally isolated box(3), freezer (4), expansion tank with coolant (5), pump (6)

In freezing, the temperature of the soil and its displacement in the radial direction were recorded. The soil temperature was measured using three thermocouples (see Fig. 4a). The first thermocouple, TC1, was attached to the copper tube to monitor the soil freezing temperature. The second thermocouple, TC2, was placed on the inner side surface of the plastic container. The third thermocouple, TC3, was attached to the strain gauge, which was placed deep into the soil sample at a height of 2.5 mm from its bottom surface and at a distance of 28 mm from the center of the plastic container. A strain gauge circuit is shown in Figure 4*b*.

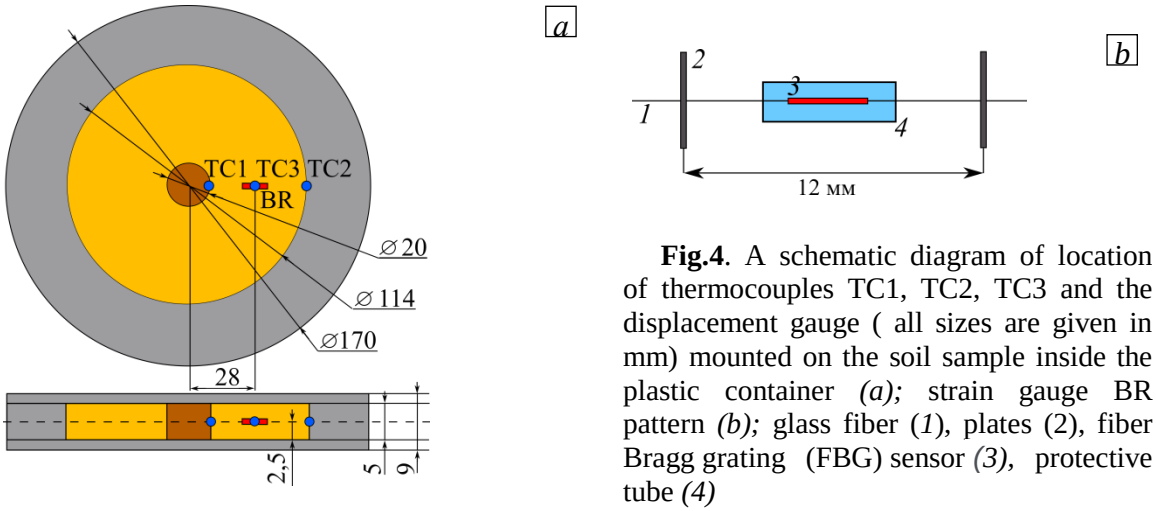

Fig.4. A schematic diagram of location of thermocouples TC1, TC2, TC3 and the displacement gauge (all sizes are given in mm) mounted on the soil sample inside the plastic container *(a);* strain gauge BR pattern *(b);* glass fiber (*1*), plates (2), fiber Bragg grating (FBG) sensor *(3),* protective tube *(4)*

It was assumed that the soil deformation caused by freezing at the points of location of the sensor plates led to their displacement, which was recorded by a sensitive element, that is, a fiber-optic sensor. To protect the sensor from the mechanical action of the soil, it was placed in a metal tube, which made it possible to prevent bending of the optical fiber at the place of its location and thus to avoid a change in the spectral picture of the signal. The temperature compensation of the readings of the fiber optic element was performed using temperature measurements obtained with a thermocouple TC3.

To meet the experimental conditions (test 2), the numerical calculation of soil freezing was carried out in an axisymmetric formulation for the rectangular region similar in size to the cross section of the plastic container z passing through the axis of rotation perpendicular to the plane of the observer (Fig.4a). The computational grid consisted of 820 quadrangular elements. The optimal mesh size was determined by analyzing the mesh convergence.

Table 3. Material parameters of quartz sand

n_0, $м^3/м^3$	ρ_s, кг/м	λ_s, Вт/(м·К)	c_s, Дж/(кг·К)	k_0, м/с	α	β	α_T, 1/К

0,35	1850	1,3	800	$3{,}5\cdot 10^{-4}$	-5,5	-12,0	$1{,}0\cdot 10^{-6}$
K_{un}, МПа	G_{un}, МПа	N_{un}, МПа	b_{un}	K_{fr}, МПа	G_{fr}, МПа	N_{fr}, МПа	b_{fr}
154	4,62	7,13	0,89	722	615	8,92	0,86

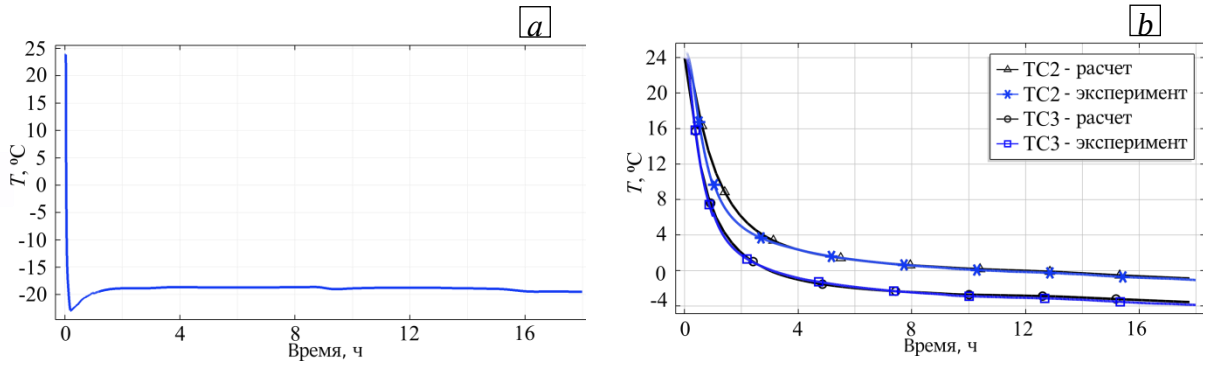

Fig.5. Time variations in the freezing temperature T_{fr}, corresponding to the recordings of thermocouple TC1 (*a*) and in the temperature T (b) measured by thermocouples TC2, TC3 and obtained in the calculation.

Thermophysical parameters for water and ice are given in Table 1, and material parameters for quartz in Table 3. The initial temperature of the soil T_0 was 24.0°C. The freezing temperature T_{fr} was set on the lateral boundary of the computational domain corresponding to the copper tube according to measurements provided by the thermocouple TC1 (Fig.5*a*.). At this boundary, the porosity n_b was supposed to be equal to $1{,}09n_0$, and the displacements were restricted in the radial direction. To calculate the heat losses, the third rank boundary conditions with the heat transfer ratio of 0.61 W/(m^2·K) were imposed on the vertical boundary of the computational domain corresponding to the lateral surface of the container and the conditions with 1,64 W/(m^2·K) and 0,9 W/(m^2·K) — on the upper and lower domain sides simulating the container lids in the calculation. The compliance of the container walls was introduced by setting the condition of an elastic constraint with the compressibility parameter of 0.72 GPa/m on the vertical boundary and of 0.12 GPa/m — on the upper and lower boundaries.

Figure 5b shows how the temperature varies with time on the external boundary of the soil sample and in the recordings made with a displacement gauge; temperature variations were measured with thermocouples TC2, TC3 and calculated numerically. It is seen that the calculated temperature graphs are in good qualitative and quantitative agreement with the curves plotted according to the results of experiment 2. A maximum discrepancy between the calculated and measured temperatures occurs at the very beginning of cooling (thermocouple TC2) and is equal to 2°C.

A minimum temperature value measured with thermocouples TC2 and TC3 is –2 and –4°C, respectively. The drop of the soil temperature from the initial value of 24°C to 0 at the point with the attached thermocouple TC3 occurs in the first 3 hours of freezing, while over the next 15 hours the temperature decreases to –4°C only. At the point with the TC2 thermocouple TC2, the soil temperature reaches 0 ° C over the period of 10.5 hours, and during the remaining 8 hours of freezing, the temperature drops only to –2°C.

The observed decrease in the freezing rate is due to an increase in the volume of the unfrozen moisture-saturated soil adjacent to the freezing front as it moves away from the freezing copper

tube. Since this leads to an increase in the heat flow to the frozen zone and the release of an additional amount of latent heat of crystallization, the propagation of the freezing front slows down.

Figure 6 contains curves showing how the radial deformation varies with time; one of these curves is plotted according to the readings of the strain gauge, and the other - according to the results of numerical simulation. The comparison of the calculated and experimental plots indicates that they are in good agreement. The analysis of the data presented allows us to draw some conclusions about the strength and deformation characteristics of frozen soils.

So, at the freezing onset, the plates of the strain sensor BR are located in the unfrozen soil zones. Due to the mechanical effect of frost heaving forces arising in the frozen zone near the copper tube, and the negative temperature deformation caused by a decrease in temperature, the unfrozen soil in these areas is compressed, as evidenced by the negative radial deformation. When the freezing front propagates to the location of the BR sensor, the volumetric expansion occurs in soil. This expansion is associated with the phase transition of pore water into ice, which is characterized by an increase in the radial deformation. After the sensor is completely located in the frozen zone, one can observe a decrease in the radial deformation caused by the compression of the already frozen soil by frost heaving forces as a reaction to restraining in case of the volumetric expansion of the newly freezing soil by the plastic container walls.

However, due to the higher rigidity of the frozen soil, the decrease in radial deformation is not as significant as at the beginning of the experiment. Note that a similar mechanical behavior of the freezing rock was recorded with strain gauges during the limestone freezing experiment [39].

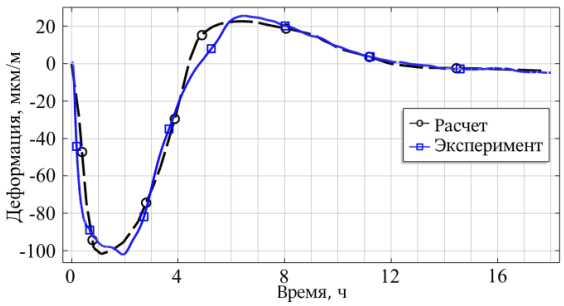

Fig. 6. Variation of radial deformation with time calculated and measured with the strain gauge BR

Unlike the one-sided soil freezing experiments which were aimed at studying the specific features of the process of soil freezing in regions with cold climates, the experimental setup described in this paper makes it possible to reconstruct the conditions for soil freezing around the freezing column used for artificial freezing of rock mass during the design and construction of underground structures. The constraints of volume expansion of the freezing soil by the plastic container simulate the situation when the soil layer artificially frozen from below and above enclosed between hard rock layers and, from the side, the movement of the soil is restrained by a surrounding unfrozen soil layer.

4. Conclusion

In this study, we have proposed a thermo-hydro-mechanical model of freezing moisture-saturated soil. The model assumes that the soil is a three-phase porous medium consisting of soil particles, liquid water and ice. The process of soil freezing is described by a system of nonlinear equations of mass transfer, heat transfer and equilibrium. To link the equations, the Clausius – Clapeyron equation, the constitutive relations of the poromechanical theory together with the effective Bishop's stress equation, as well as the empirical dependences of ice saturation, moisture conductivity, thermophysical and mechanical properties on temperature and porosity are used. In addition, the model includes an associated plastic flow law for calculating the inelastic volumetric deformation that occurs when the soil is stretched under the influence of the pore pressure of ice. The model is implemented and executed in the finite element software package Comsol Multiphysics® using standard interfaces. The validity of the developed thermo-hydro-mechanical model for describing moisture-saturated soil freezing is demonstrated by the numerical simulation of two laboratory experiments at different freezing temperatures. The results obtained show:

– in laboratory test 1 on one-sided freezing of silty clay samples subjected to varying vertical loads in an open system at two temperature regimes conditions, the model allowed us to simulate

the temporal evolution of temperature inside the sample and the growth of the absolute value of soil frost heave deformation with time until the temperature stabilized. It was found that when the soil sample freezing is accompanied by the formation of a massive cryogenic structure in the absence of thick ice lenses, the numerical simulation more accurately predicts the magnitude of the absolute deformation of frost heaving in comparison with the soil freezing process involving the formation of thick ice lenses;

– in laboratory test 2 on radial freezing of moisture-saturated sand in confined conditions, the model made it possible to predict the temperature change in the soil with time and the nature of its deformation. It was found that the calculated and experimental curves showing the temperature variation with time at points of the soil located inside the sample and at its boundary are in good agreement. The curve of soil deformation in the radial direction during freezing, established by numerical simulation, quite accurately describes the measurements made with a fiber-optic sensor. It is shown that at the same time the quantitative discrepancy between the calculated and experimental curves increases at the beginning of freezing and at the local transition of the soil from the state of compression to the state of tension.

Theoretical studies presented in Sections 2 and 3.1 was funded by RFBR, project number 19-31-90107; experimental studies presented Section 3.2 was funded by the Ministry of Education and Science of the Perm Krai (agreement No. C-26/563 dated March 23, 2021).

References

1. Kiselev M.F. *Preduprezhdeniye deformatsii gruntov ot moroznogo pucheniya* [Prevention of ground deformation from frost heave]. Leningrad, Stroyizdat. Leningr. otd-niye, 1985. 130 p.
2. *Tayukin G.I., Fursov V.V., Balura M.V.* Seasonal soil freezing impact on foundations of buildings (liquefied hydrocarbon depot terminal). *Vestnik Tomskogo gosudarstvennogo arkhitekturno-stroitel'nogo universiteta – Journal of Construction and Architecture*, 2019, no. 6, pp. 186-198. https://doi.org/10.31675/1607-1859-2019-21-6-186-198
3. Yang B., Qin Z., Zhou Q., Li H., Li L., Yang X. Pavement damage behaviour of urban roads in seasonally frozen saline ground regions. *Cold Regions Sci. Tech.*, 2020, vol. 174, 103035. https://doi.org/10.1016/j.coldregions.2020.103035
4. Long X., Cen G., Cai L., Chen Y. Model experiment of uneven frost heave of airport pavement structure on coarse-grained soils foundation. *Construct. Build. Mater.*, 2018, vol. 188, pp. 372-380. https://doi.org/10.1016/j.conbuildmat.2018.08.100
5. Gorelik J.B. Metody rascheta deformatsiy inzhenernykh konstruktsiy, vyzvannykh pucheniyem porod promerzayushchego sloya [On the calculation methods of the engineering construction displacements caused by freezing layer frost heave process]. *Kriosfera Zemli – Earth's Cryosphere*, 2010, vol. 14, no. 1, pp. 50-62.
6. Teng Z.-C., Liu X.-Y., Liu Y., Zhao Y.-X., Liu K.-Q., Teng Y.-C. Stress–strain assessments for buried oil pipelines under freeze-thaw cyclic conditions. *J. Pressure Vessel Technol.*, 2021, vol. 143(4), 041803. https://doi.org/10.1115/1.4049712
7. Cai H., Li S., Liang Y., Yao Z., Cheng H. Model test and numerical simulation of frost heave during twin-tunnel construction using artificial ground-freezing technique. *Computers and Geotechnics*, 2019, vol. 115, 103155. https://doi.org/10.1016/j.compgeo.2019.103155
8. Zhou J., Zhao W., Tang Y. Practical prediction method on frost heave of soft clay in artificial ground freezing with field experiment. *Tunnelling and Underground Space Technology*, 2021, vol. 107, 103647. https://doi.org/10.1016/j.tust.2020.103647
9. Khakimov Kh.R. *Voprosy teorii i praktiki iskusstvennogo zamorazhivaniya gruntov* [Problems in the theory and practice of artificial freezing of soil]. Moscow, Izd-vo Akad. nauk SSSR, 1957. 191 p.
10. *Orlov V.O., Kim V.K.* A method of evaluating the frost-heave pressure of soil against the ice-soil enclosure of an underground structure. *Soil Mech. Found. Eng.*, 1988, vol. 25, pp. 129-135. https://doi.org/10.1007/BF01709718
11. Ji Y., Zhou G., Hall M.R. Frost heave and frost heaving-induced pressure under various restraints and thermal gradients during the coupled thermal–hydro processes in freezing soil. *Bull. Eng. Geol. Environ.*, 2019, vol. 78, pp. 3671-3683. https://doi.org/10.1007/s10064-018-1345-z
12. Sumgin M.I. *Fiziko-mekhanicheskiye protsessy vo vlazhnykh i merzlykh gruntakh v svyazi s obrazovaniyem puchin na dorogakh* [Physical and mechanical processes in wet and frozen soils in connection with the formation of abyss on the roads]. Moscow, Transpechat' NKPS, 1929. 592 p.
13. Taber S. Frost heaving. *J. Geol.*, 1929, vol. 37, no. 5, pp. 428-461.
14. Taber S. The mechanics of frost heaving. *J. Geol.*, 1930, vol. 38, no. 4, pp. 303-317.
15. Tsytovich N.A. *The mechanics of frozen ground*. McGraw-Hill, 1975. 426 p.

16. Hoekstra P. Moisture movement in soils under temperature gradients with the cold-side temperature below freezing. *Water Resour. Res.*, 1966, vol. 2, pp. 241-250. https://doi.org/10.1029/WR002i002p00241
17. Penner E., Gold L.W. Transfer of heaving forces by adfreezing to columns and foundation walls in frost-susceptible soils. *Canadian Geotechnical Journal*, 1971, vol. 8, pp. 514-526. https://doi.org/10.1139/t71-053
18. Ivanov N.S. *Teplo- i massoperenos v merzlykh gornykh porodakh* [Heat and mass transfer in frozen ground]. Moscow, Nauka, 1969. 240 p.
19. Harlan R.L. Analysis of coupled heat-fluid transport in partially frozen soil. *Water Resour. Res.*, 1973, vol. 9, pp. 1314-1323. https://doi.org/10.1029/WR009i005p01314
20. O'Neill K., Miller R.D. Exploration of a rigid ice model of frost heave. *Water Resour. Res.*, 1985, vol. 21, pp. 281-296. https://doi.org/10.1029/WR021i003p00281
21. Coussy O. Poromechanics of freezing materials. *J. Mech. Phys. Solid.*, 2005, vol. 53, pp. 1689-1718. https://doi.org/10.1016/j.jmps.2005.04.001
22. Zhou M.M., Meschke G. A three-phase thermo-hydro-mechanical finite element model for freezing soils. *Int. J. Numer. Anal. Meth. Geomech.*, 2013, vol. 37, pp. 3173-3193. https://doi.org/10.1002/nag.2184
23. Tounsi H., Rouabhi, A., Tijani M., Guérin F. Thermo-hydro-mechanical modeling of artificial ground freezing: Application in mining engineering. *Rock Mech. Rock Eng.*, 2019, vol. 52, pp. 3889-3907. https://doi.org/10.1007/s00603-019-01786-9
24. Nishimura S., Gens A., Olivella S., Jardine R.J. THM-coupled finite element analysis of frozen soil: Formulation and application. *Géotechnique*, 2009, vol. 59, pp. 159-171. https://doi.org/10.1680/geot.2009.59.3.159
25. Ghoreishian Amiri S.A., Grimstad G., Kadivar M., Nordal S. Constitutive model for rate-independent behavior of saturated frozen soils. *Canadian Geotechnical Journal*, 2016, vol. 53, pp. 1646-1657. https://doi.org/10.1139/cgj-2015-0467
26. Zhou J., Li D. Numerical analysis of coupled water, heat and stress in saturated freezing soil. *Cold Regions Sci. Tech.*, 2012, vol. 72, pp. 43-49. https://doi.org/10.1016/j.coldregions.2011.11.006
27. Lai Y., Pei W., Zhang M., Zhou J. Study on theory model of hydro-thermal-mechanical interaction process in saturated freezing silty soil. *Int. J. Heat Mass Tran.*, 2014, vol. 78, pp. 805-819. https://doi.org/10.1016/j.ijheatmasstransfer.2014.07.035
28. Arzanfudi M.M., Al-Khoury R. Freezing-thawing of porous media: An extended finite element approach for soil freezing and thawing. *Adv. Water Resour.*, 2018, vol. 119, pp. 210-226. https://doi.org/10.1016/j.advwatres.2018.07.013
29. Kosheleva N.A., Serovaev G.S. Modeling a stressed state in the vicinity of an optical fiber embedded in a polymer composite material with allowance for the structural features of the composite. *J. Appl. Mech. Tech. Phy.*, 2018, vol. 59, pp. 1271-1278. https://doi.org/10.1134/S0021894418070088
30. Fedorov A.Y., Kosheleva N.A., Matveenko V.P., Serovaev G.S. Strain measurement and stress analysis in the vicinity of a fiber Bragg grating sensor embedded in a composite material. *Compos. Struct.*, 2020, vol. 239, 111844. https://doi.org/10.1016/j.compstruct.2019.111844
31. Ren G., Li T., Hu Z., Zhang C. Research on new FBG soil pressure sensor and its application in engineering. *Optik*, 2019, vol. 185, pp. 759-771. https://doi.org/10.1016/j.ijleo.2019.03.019
32. Zhelnin M.S., Prokhorov A.E., Kostina A.A., Plekhov O.A. Experimental and theoretical study of mechanical deformation of freezing saturated soil. *Vestnik PNIPU. Mekhanika – PNRPU Mechanics Bulletin*, 2019, no. 4, pp. 19-28. https://doi.org/10.15593/perm.mech/2019.4.02
33. Zhao X., Lv X., Wang L., Zhu Y., Dong H., Chen W., Li J., Ji B., Ding Y. Research of concrete residual strains monitoring based on WLI and FBG following exposure to freeze-thaw tests. *Cold Regions Sci. Tech.*, 2015, vol. 116, pp. 40-48. https://doi.org/10.1016/j.coldregions.2015.04.007
34. Wang M., Li X., Chen L., Hou S., Wu G., Deng Z. A modified soil water content measurement technique using actively heated fiber optic sensor. *Journal of Rock Mechanics and Geotechnical Engineering*, 2020, vol. 12, pp. 608-619. https://doi.org/10.1016/j.jrmge.2019.11.003
35. Sun M.-Y., Shi B., Zhang D., Liu J., Guo J.Y., Wei G.-Q., Cheng W. Study on calibration model of soil water content based on actively heated fiber-optic FBG method in the in-situ test. *Measurement*, 2020, vol. 165, 108176. https://doi.org/10.1016/j.measurement.2020.108176
36. Thomas H.R., Cleall P., Li Y.-C., Harris C., Kern-Luetschg M. Modelling of cryogenic processes in permafrost and seasonally frozen soils. *Géotechnique*, 2009, vol. 59, pp. 173-184. https://doi.org/10.1680/geot.2009.59.3.173
37. Nixon J.F. Discrete ice lens theory for frost heave in soils. *Canadian Geotechnical Journal*, 1991, vol. 28, pp. 843-859. https://doi.org/10.1139/t91-102
38. Mu S., Ladanyi B. Modelling of coupled heat, moisture and stress field in freezing soil. *Cold Regions Sci. Tech.*, 1987, vol. 14, pp. 237-246. https://doi.org/10.1016/0165-232X(87)90016-4
39. Tounsi H., Rouabhi A., Jahangir E. Thermo-hydro-mechanical modeling of artificial ground freezing taking into account the salinity of the saturating fluid. *Computers and Geotechnics*, 2020, vol. 119, 103382. https://doi.org/10.1016/j.compgeo.2019.103382

The authors declare no conflict of interests.

The original paper was received on 14.04.2021 and published in Russian on 28.04.2021.